Confined Crystallization of Ethylene Oxide−Butadiene Diblock Copolymers in Lamellar Films

Ricarda Opitz, Denitza M. Lambreva, and Wim H. de Jeu*

FOM-Institute AMOLF, Kruislaan 407, 1098 SJ Amsterdam, The Netherlands

Received March 11, 2002

ABSTRACT: The isothermal crystallization of a semicrystalline poly(ethylene oxide-*b*-ethylene/butylene) diblock copolymer (PEO-*b*-PB$_h$) in uniform lamellar films has been investigated by X-ray reflectivity, optical microscopy, and atomic force microscopy. Crystallization of the PEO block leads to an increase in the lamellar thickness of both blocks. As the density of PEO increases upon crystallization, this effect is accompanied by a contraction in the lateral direction, which results in cracking of the film. The combination of the different techniques allows construction of a complete model with an integer or half-integer number of folds in the vertically oriented crystalline stems.

Introduction

The knowledge of polymer crystallization and the resulting morphology is a key to understanding many aspects of polymer ordering and self-assembly. The chain folding that usually accompanies polymer crystallization[1,2] depends strongly on the kinetic pathways of the process. The crystallization conditions essentially determine the degree of crystallinity, the final microstructure, and supermolecular structures like spherulites. Recent progress in understanding polymer crystallization regards advanced techniques indicating preordering in the early stages of the process. Though the exact nature of these effects is still a matter of considerable debate,[2−4] some form of consensus has evolved about the existence of local orientational ordering of the polymer chains as a basis for the formation of a nucleus. In addition, computer simulations have also strongly challenged some of the accepted textbook ideas about the onset of crystallization.[5,6] In this context the application of external "fields" exerted by pressure, shear flow, or well-defined boundary conditions provides a means to influence and possibly to control the pathways to nucleation and chain folding. One possibility to be explored in this paper is the use of uniformly aligned lamellar block copolymer films of poly(ethylene oxide-*b*-ethylene/butylene) (PEO-*b*-PB$_h$) to confine the crystallization process of the PEO blocks.

In a diblock copolymer the interaction between the chemically distinct blocks leads below the order−disorder transition temperature (ODT) to microphase separation.[7] If one of the blocks is semicrystalline, a specific situation occurs of confined crystallization within the microphase-separated morphology. Interestingly, in such a system equilibrium chain folding can be achieved.[8−10] A structure of alternating amorphous and crystalline layers has been predicted, the latter with regular chain folding with the chain stems perpendicular to the interface. The alternative situation of extended crystallized chains cannot be an equilibrium situation (as is the case for homopolymers) as it would lead to a strongly increased entropy due to the necessarily accompanying stretching of the chains of the amorphous block.

Bulk investigations of diblock copolymer systems with one crystallizable block are numerous and have been reviewed.[11] In the present context especially recent work involving PEO is of interest. Crystallization in a series of PEO-*b*-PBO [poly(butylene oxide)] and PEO-*b*-PPO [poly(propylene oxide)] was studied by Ryan and co-workers.[12−15] Cheng and co-workers[16,17] investigated the PEO-*b*-PS system. The confined surroundings have a profound influence on the crystallization properties. The relations between the ODT, the crystallization temperature T_{cr} of PEO, and the glass transition temperature T_g of the noncrystallizable block are of decisive importance. In the case of PEO-*b*-PS, PEO crystallization from a microphase-separated melt takes place between hard glassy PS boundaries. Depending on the morphology, this can lead to a "breaking out" of the crystalline structure from the original morphology, which is destroyed. Alternatively, for $T_g < T_{cr}$ confined crystallization develops between "rubbery" boundaries. If on the temperature scale the ODT and T_{cr} are close, further complications occur.

Despite the extensive bulk work, far less is known about confined crystallization in thin films. Of special interest is the situation of about equal volume fractions of the blocks, which gives below the ODT rise to a lamellar structure. The randomly oriented lamellar microdomains become macroscopic lamellae under the influence of surfaces. These systems have been well studied[18] because of their various applications in materials science as well as the interest from the point of view of fundamental research. In the lamellar morphology thin block copolymer films provide a precise control of the boundary conditions over macroscopic areas. We used a symmetrical PEO-*b*-PB$_h$ diblock copolymer, which was isothermally crystallized from the ordered melt. This corresponds to the situation of "rubbery" confinement mentioned above. Before and after the crystallization a well-ordered layered system is found, in the latter situation corresponding to alternating crystallized and amorphous blocks. The film are investigated with optical and atomic force microscopy and X-ray reflectivity techniques. While the first techniques provide surface information, the latter allows a quantitative determination of the changes in the various (sub)layers throughout the film upon crystallization. Crystallization leads despite the increased density to

* Corresponding author: e-mail dejeu@amolf.nl.
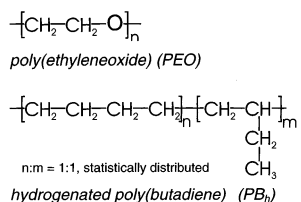
Figure 1. Chemical structures of poly(ethylene oxide) and hydrogenated poly(butadiene).

Table 1. Characteristics of the Diblock Copolymers

	PEO	PBh
M_n (g/mol)	4300	3700
no. of monomers N	98	66
vol fraction f^a	0.46	0.54
radius of gyration (nm)	1.1	1.3
length of nonfolded block (nm)	27.4	25.4
polydispersity	1.02	

^{a} Calculated from $f_{PEO} = N^*_{PEO}/(N^*_{PEO} + N^*_{PBh})$, with $N^*_{PEO} + N^*_{PBh} = N_{PEO}(\rho_{PBh}/\rho_{PEO}) + N_{PBh}(\rho_{PEO}/\rho_{PBh})$. Here ρ is the density for which $\rho_{PEO} = 1.13$ g/cm^3 and $\rho_{PBh} = 0.86$ g/cm^3 were used.

an increased PEO block thickness. The increase is such that an integer or half-integer ratio between the lamellar thickness and the total block length can be reached. To conserve density, an attendant stretching of the PB block takes place. The total stretching causes a lateral contraction through the whole film, leading to the formation of holes and cracks.

Experimental Section

Materials. An approximately symmetric PEO-*b*-PB$_h$ diblock copolymer (Figure 1) was obtained from Goldschmidt AG (Essen, Germany). Synthesis was done by sequential anionic polymerization of butadiene (about 50% 1,4 and 50% 1,2 addition, statistically distributed) and ethylene oxide. The PB$_h$ block was obtained by hydrogenation of poly(butadiene). The characteristics of the block polymer are given in Table 1. Before use, the polymer was dried under vacuum at 80 °C to remove the solvent. The PEO block is terminated by an OH group. To compare the influence of different end groups, part of the block copolymer was methylated. The subsequent sample treatment was identical to that of the hydroxy-terminated block copolymer.

Films were obtained by spin-coating a block copolymer solution in dichloromethane onto silicon wafers at 2000 rpm. The film thickness was tuned by variation of the concentration and the rotation speed. The initial thickness was approximately 150 nm. Samples were mounted in a temperature-controlled two-stage oven and evacuated to <10^3 Pa in order to provide environmental control and reduce air scattering. The temperature was controlled with an accuracy of 0.1 °C by a Eurotherm controller. A separate thermocouple close to the sample allowed reading the sample temperature precisely. A standard procedure was used for annealing and cooling the films. The samples were first annealed at $T_{ann} = 90$ °C, well above the bulk melting temperature of about 60 °C. Equilibrium throughout the whole stack of layers was reached after about 3 h, as evidenced by X-ray reflectivity. Cooling to T_{cr} was realized by fluxing the outside of the oven with nitrogen gas from a container with liquid nitrogen. In this way cooling rates of 10 °C/min were achieved. In the case of small supercooling (40 and 45 °C) some crystals were "seeded" by first cooling to about 30 °C before returning to the chosen value of T_{cr}.

Optical Microscopy. Optical images of the film surface were obtained in a nitrogen atmosphere using a Leitz Ortho-plan microscope equipped with a Linkam THMS600 hot stage. Samples were molten at 90 °C and isothermally crystallized at various temperatures. For small supercooling nucleation is very slow, and temperature jumps were performed to about
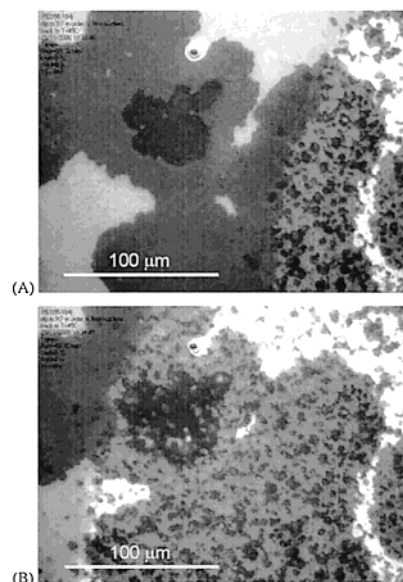
Figure 2. Optical microscopy of isothermal crystallization of a film at 45 °C. (A) Left: well-ordered terraces of the molten lamellar structure. Right: crystallization front moving over the film from the right side. (B) Same area 1 min later; the crystallization front has almost crossed the full window.

30 °C in order to "seed" a nucleus. All images were taken in reflection using a white light source in order to obtain interference colors. Images of the displacement of the crystalization front were captured in real time using a CCD camera.

Atomic Force Microscopy. Once the crystallization at the selected temperature was completed, the surface morphology of the block copolymer films was investigated by atomic force microscopy (AFM) at ambient conditions using a Solver AFM from NT-MDT (Zelenograd, Moscow). A vibrating cantilever with a resonant frequency of about 300 kHz and a silicon tip with a curvature radius ≤10 nm was used as a probe, allowing simultaneous detection of the height profile and the corresponding phase contrast. The lateral and vertical resolutions were about 20 and 0.2 nm, respectively.

X-ray Reflectivity. To perform X-ray reflectivity measurements, the samples were placed vertically on a two-circle diffractometer attached to a Rigaku RU-300H rotating-anode generator operated at 18 kW. The incident beam was monochromatized to $\lambda = 0.154$ nm (Cu Kα line) and converted into an approximately parallel beam by a W/B$_4$C graded parabolic multilayer mirror. The mirror provides a beam with an intrinsic divergence of about 25 mdeg in the horizontal scattering plane (*xz*-plane with the *z*-axis along the film normal). Additional presample and predetector slits lead to an overall in-plane resolution given by $\Delta q_z = 0.043$ nm^{-1} and $\Delta q_x = (5 \times 10^{-3}) q_z$.

In reciprocal space specular scans probe the scattered intensity along q_z. The reflected X-ray intensity was corrected for sample size effects at small incidence angles as well as for background scattering; the incident intensity was normalized to unity. The data were analyzed using an iterative matrix formalism derived from the Fresnel equations, taking the deviations into account from the ideal decay of the reflectivity for a perfectly smooth surface due to the presence of roughness.[19,20] The calculated reflectivity profiles were convoluted with the experimental resolution, assumed to be of Gaussian statistics.

Results

An overview of the dynamics at the surface during crystallization is given by the optical micrographs in Figure 2. At the surface of the PEO-*b*-PB$_h$ film two different regions corresponding to the molten and the crystallized structure can easily be distinguished. In the

(A)

(B)
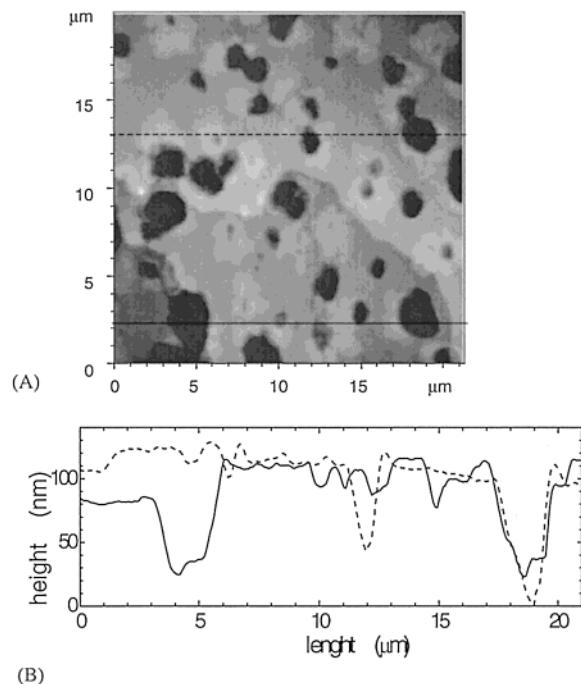
Figure 3. AFM picture of a film in the crystallized state. (A) Height picture with terrace structure and deep holes formed during crystallization. (B) Height profiles along the two lines indicated in (A).

melt (here at $T = 45$ °C) at the left and middle part of Figure 2A, the typical terrace structure of a lamellar block copolymer film is visible.[7,21−23] Different gray scales indicate three distinct levels, which differ in height by a full block period. After a nucleus has been formed, the crystallization front moves laterally over the film (compare parts A and B of Figure 2). As reported earlier for a very similar block copolymer system,[11,23] during this process the different height levels are preserved: evidently, crystallization does not destroy the lamellar film structure parallel to the substrate. The crystallization front is characterized by a depletion zone at its front and leaves a cracked film surface behind. An increase of the total film thickness is evident from the lighter color of the terraces. Hence, material is pulled out locally and rearranged vertically during the process of crystal formation. The lamellar thickness increases and the film cracks. In fact, some holes appear already in the depletion zone.

The depth of the cracks after crystallization has been investigated by AFM. Figure 3A shows a $\times 20$ μm^2 detail of the surface of the same film; height profiles along the two lines are displayed in Figure 3B. The terrace structure with distinct steps is very clear, while also holes due to the cracking of the film can be quantified. Some of the cracks extend deep and occasionally even go through the whole film down to the substrate. The AFM pictures allow an approximate quantification of the various levels involved. The terrace height, which coincides with the lamellar period L, is after crystallization about 20 nm, while the total film thickness D amounts to approximately 110 nm. From these results we preliminary conclude for this crystallized film to an asymmetric morphology with 5.5 periods. In the depth profiles of the cracks multiples of L can clearly be seen; however, in some cases also values around $L/2$ appear.

In contrast to AFM, X-ray reflectivity turns out to be well-suited to obtain a more complete quantification of

(A)

(B)
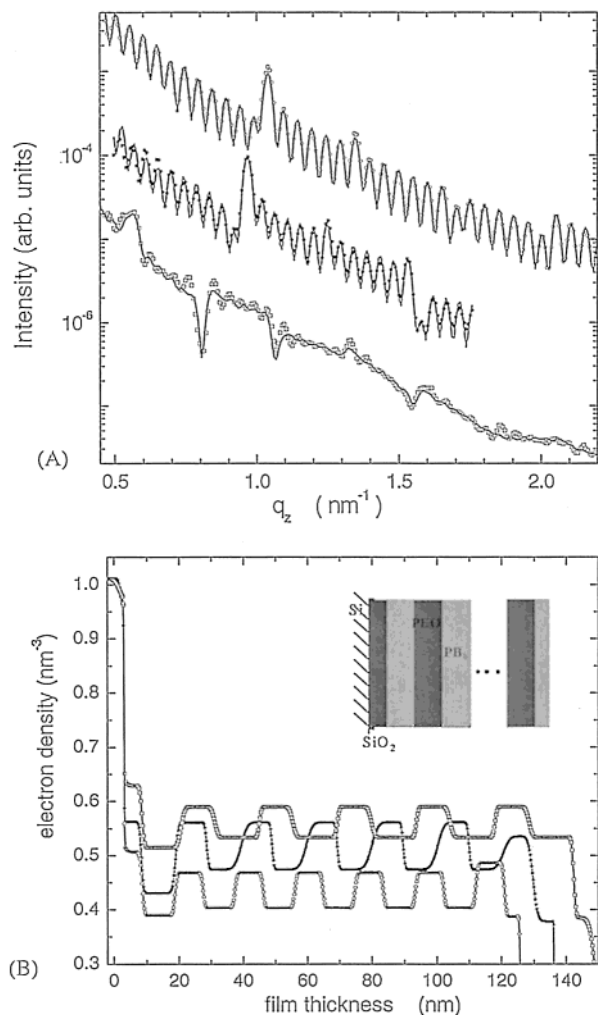
Figure 4. (A) Specular X-ray reflectivity of a 6.5 layer film with best fit to the data as full lines; curves have been shifted for clarity. (B) Associated electron density profiles with as inset the stack model. Open circles, molten state at $T = 90$ °C; filled dots, melt at $T = 45$ °C; open squares, $T = 45$ °C after crystallization.

the structural properties of our block copolymer films. Measurements were taken in dependence of the annealing temperature and the different crystallization temperatures. As an example, Figure 4A shows a full series of X-ray reflectivity curves with their respective fittings. The upper curve depicts the measurement of a 6.5 layer film at $T = T_{ann} = 90$ °C in the molten phase-separated state. Besides the so-called Kiessig fringes, which indicate the total film thickness, several orders of Bragg peaks are visible. Hence, we can conclude to a rather perfect lamellar ordering of alternating layers of PEO and PB_h oriented parallel to the substrate. Precise results are obtained by fitting the experimental curves to the model sketched in the inset of Figure 4B. As shown in Figure 4A by the solid lines, a good agreement between experimental and model data could be achieved. Not including the SiO_x layer on top of the substrate, the total film thickness is given by $D = 122.9 \pm 0.1$ nm and the lamellar period by $L = 18.7 \pm 0.1$ nm, which is close to 6.5 layers. The density profiles in Figure 4B reflect the thickness, the roughness at the interfaces, and the electron densities of the substrate, SiO_x, PEO, and PB_h layers. In the fitting commonly used values for the dispersion and the absorption of the Si substrate and the oxide layer were kept as fixed parameters; they were

**Table 2. Fitting Results of the X-ray Reflectivity (Error Bars for the (Sub)layer Thickness Are ±0.1 nm)**

	amorphous		crystalline				
	90 °C	45 °C	45 °C	40 °C	35 °C	30 °C	25 °C
film thickness D (nm)	123	133	152	163	130	137	134
d_{PEO} in period (nm)	8.8	9.7	10.4	8.9	9.1	7.9	8.3
d_{PBh} in period (nm)	9.9	10.6	13.8	13.3	11.9	12.9	11.7
$L = d_{PEO} + d_{PBh}$ (nm)	18.7	20.3	24.2	22.2	20.9	20.7	20.1
D/L	6.6	6.5	6.3	7.4	6.2	6.6	6.6
$27.4/d_{PEO}$			2.62	3.07	3.02	3.49	3.29
no. of stems			2.5/5	3/6	3/6	3.5/7	3.5/7

based on mass densities of 2.33 g/cm^3 for Si and 2.23 g/cm^3 for SiO$_x$.

It should be mentioned that several problems still exist in the fitting of the X-ray reflectivity. In the first place the structure of the toplayers can only be determined in an approximate average way. The noncomplete filling associated with to the structure of different levels on top of the film is expressed only as a decreased electron density of the last PB$_h$ layers near the air interface. Figure 4A shows that the fitting over the limited q range measured is rather good. Hence, introducing further modeling of the top layers will hardly increase the quality of the fit and would lead to inaccurate additional parameters. Second, the mosaic of the film as obtained from rocking curves showed at low q values some structure. Therefore, the absolute values of the densities have to be treated with caution. The repeated thicknesses in the central part of the film, which are our main concern in discussing the crystallization process, appear to be hardly sensitive to these details of the fitting. They are given in Table 2 together with their relation to the extended chain length of PEO.

Lowering the temperature to the crystallization point (here T = 45 °C) does not immediately result in crystallization of the sample: until a nucleus is formed, the system stays in the molten state. Further stretching of the polymer chains occurs leading to an increase in the lamellar period.[24,25] In the middle curve of Figure 4A this is reflected by a shift in the Bragg position to smaller q_z values, while the basic features of the curve are preserved. From the fitting we find now L = 20.3 nm and D = 133.0 nm. The corresponding profile in Figure 4B indicates that the thickness of both the PEO and the PB$_h$ layers have increased. In addition, strong changes are observed in the top layers. Evidently, the increase of the lamellar period results in a reorganization of material in the sense that some of the upper islands disappear and new holes are created.

After formation of a nucleus, crystallization proceeds laterally over the sample. Once this process is finished and the sample remains stable over a prolonged period, the lower curve of Figure 4A results. Now the general features have changed drastically. First, the Bragg positions have further decreased, indicating another increase in the lamellar thickness. Second, also the phase of the peaks has changed leading to "negative" peaks in the crystallized state. This effect is directly connected to a change in the ratio of the two block electron densities from ρ_{e-PEO}/ρ_{e-PB} = 1.16 in the melt at 90 °C to 1.18 at 45 °C before and finally to 1.11 after the crystallization. Furthermore, the amplitude of the Kiessig fringes has decreased, and the decay of the whole reflectivity curve has become stronger, due to an increased roughness both at the surfaces and at the interfaces. From the fitting we obtain at T_{cr} = 45 °C a lamellar period of L = 24.1 ± 0.1 nm. At the substrate we find a PEO layer with the thickness of 5.5 nm, which
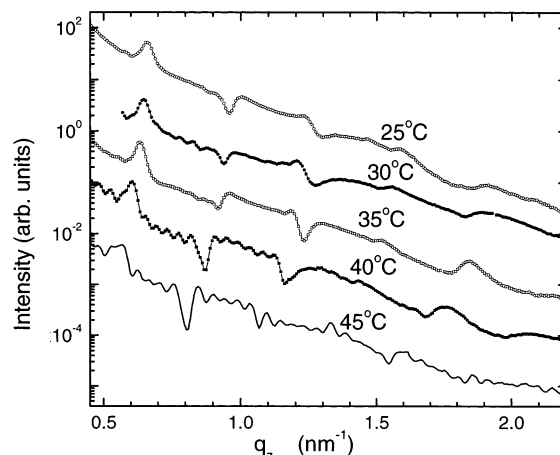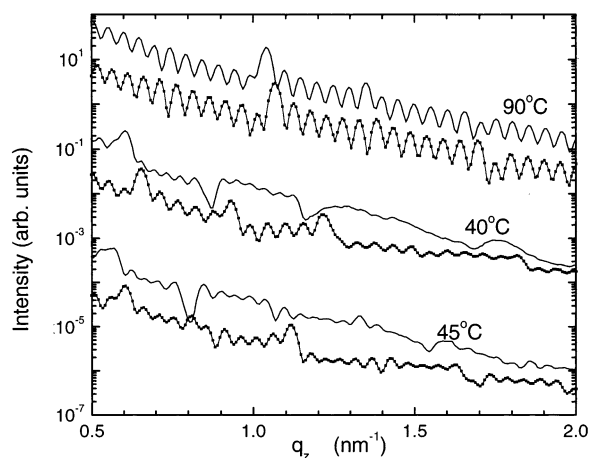

Figure 5. Specular X-ray reflectivity after isothermal crystallization at different temperatures. The curves have been shifted for clarity.
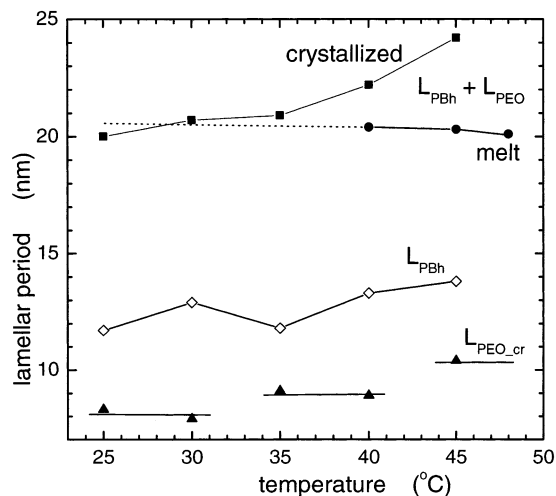
Figure 6. Lamellar period L and sublayer thicknesses at various temperatures as determined by fitting the X-ray reflectivity.

coincides with a 4 times folded chain, consisting of five vertical stems. In the stack of layers the fitting results in a PEO sublayer thickness of 10.1 nm, slightly less than twice the value of the layer at the substrate. A discussion follows in the next paragraph. In Table 2 the results at all five different crystallization temperatures (45, 40, 35, 30, and 25 °C) are given. The values for the (sub)layer spacings at these temperatures are compared in Figure 6.

Finally, in Figure 7 the samples with the hydroxy- and the methyl-terminated end groups are shown for three different temperatures. In the melt at T_{ann} = 90 °C the features of both curves are essentially the same, the difference being a smaller lamellar period for the methylated sample. From the fitting we obtain

Figure 7. Specular X-ray reflectivity of block copolymer films with OH-terminated end groups (full lines) and CH₃-terminated end groups (squares), in the melt (90 °C) and after crystallization. The curves have been shifted for clarity.

L(me) = 18.3 ± 0.1 nm and L_{PEO}(me) = 8.6 ± 0.1 nm. The same tendency of a smaller lamellar period for the methyl-terminated PEO block is found for the crystallized samples at 40 and 45 °C. As the general features are not different from the samples with a hydroxy termination, we shall not go into further details.

Discussion

Lamellar Structure. Preferential block segregation necessary of block copolymers at interfaces leads to films with a thickness quantified as $D = (n + 1/2)L$ (asymmetric layer stacking) or $D = nL$ (symmetric layer stacking), where L is the lamellar period and n is an integer.[21,26,27] In both cases the top and bottom layer have in principle half the thickness of the corresponding interior layers of the film. From the X-ray results in Figure 4 and Table 2, our samples evidently have an asymmetric lamellar geometry, confirming the AFM picture. The block with the larger electron density is situated at the substrate on top of the SiO_x layer, while the low-density layer forms the interface to the air. Also, the factor of 2 between the thickness of the interior and the outermost layers is reasonably well reproduced. The asymmetric layer stacking contradicts some microscopy studies of thin PEO-*b*-PB$_h$ films,[22,23] in which the authors conclude to a symmetric configuration with PB$_h$ at both outer interfaces. In fact, these latter results are somewhat counterintuitive, as PEO is expected to be more compatible to a SiO_x layer than the nonpolar PB$_h$. More importantly, compared to optical microscopy, which gives only an approximate value for the thickness, X-ray reflectivity determines the thickness of the single sublayers with high precision.

If the initial film thickness is somewhat larger than the quantized value, islands form at the surface; if the film is somewhat short of material, holes appear. These islands and holes have a height *cq* depth equal to the full block period L. They can be seen as different uniform gray levels in our microscopic pictures (Figures 2 and 3). In fact, the situation is somewhat more complicated as three levels have been observed, which in principle would be also possible for a precise quantized thickness. In the modeling of the reflected X-ray intensity this shows up as an increased surface roughness and a diminished electron density of the top layers.

Chain Stretching. SAXS experiments on the same polymer in bulk indicate a strong temperature dependence of the lamellar period.[28] In the melt an increase is observed from $L = 15.3$ nm at 250 °C to $L = 18.5$ nm at 90 °C. As it is not possible to reach the ODT, no reference value at the phase transition is available. For a Gaussian coil with a radius of gyration $R_G = a\sqrt{N/6}$,[7] where N is the degree of polymerization and the monomer unit lengths are $a_{\text{PEO}} = 0.280$ nm and $a_{\text{PBh}} = 0.385$ nm, a lamellar period of 9.6 nm would be obtained. Compared to this situation, at 90 °C the molecules in the lamellae are stretched by almost a factor of 2. The experimental values for the two sublayers of Table 2 can be well approximated by splitting L according to the volume fractions of PEO and PB$_h$. The same holds at 45 °C, for both the melt and the crystallized state. In the latter situation the volume fraction of PEO must be corrected for the change in density from amorphous (1.125 g/cm³) to crystalline (1.225 g/cm³).

Upon crystallization, the lamellar period increases despite the decreasing volume (increasing density) of PEO. The only possibility seems to attribute this expansion to the need to fit the thickness of the PEO sublayer to an integer (or half-integer) number of stems. Density conservation forces the PB$_h$ block to follow this stretching. Evidently, the loss of entropy associated with the PB$_h$ stretching is more than compensated by the favorable packing of the PEO stems. As a consequence, a lateral contraction results through the whole film. Implicit in this interpretation is that the folded PEO
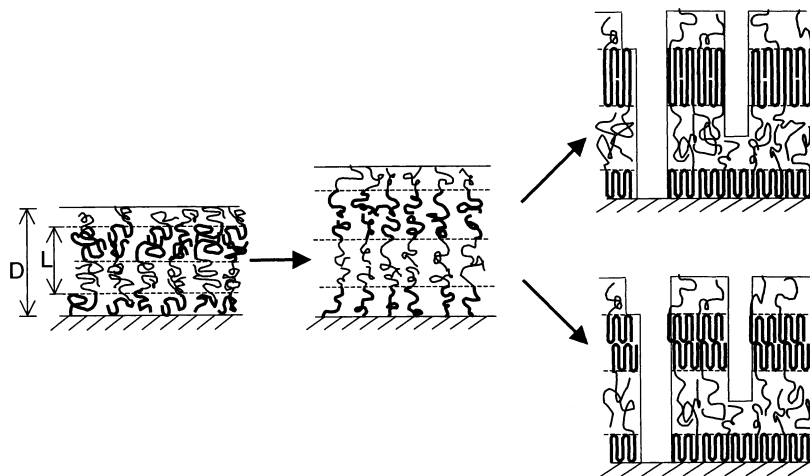
Figure 8. Model for the development of the layer structure and the polymer folds during crystallization.

chains are perpendicular to the layers. Though we do not have direct proof for this statement, there is considerable circumstantial evidence: (1) The block segregation implies that the chains are oriented perpendicular to the interfaces in order to minimize the contact area. (2) If the chains were tilted with respect to the interface normal, a simple variation in the tilt angle could accommodate the increased length without PB_h stretching and lateral shrinkage. Finally, we note that Hong et al.[23] have explicitly observed perpendicular chains in related (nonhydrogenated) PEO-*b*-PB films by electron diffraction.

Cocrystallization. Modern ideas about the early stages of crystallization assume local "embryos" of ordered stems.[4] In this context the present situation of uniform stretching of the chains provides a perfect preconditioning to crystallization. Hence, we anticipate a somewhat larger degree of crystallization than the approximately 85% in the bulk.[22] In principle, the degree of crystallinity in a film could be obtained from a measurement of the critical angle in X-ray reflectivity, which determines the average density. However, this approach is precluded by the unknown contribution to the density from the voids due to the lateral expansion upon crystallization.

To determine the number of stems at the various temperatures, we can take the extended chain length for PEO from Table 1, divide it by the number $n = 2, 3, ...$, and compare with the PEO sublayer thickness. For the PEO layer at the substrate this leads with decreasing temperature to $n = 5, 6$, and 7 stems. For the interior PEO layers of the film the same number of folds as in the bottom layer would lead to a crystalline double layer (see Table 2 and Figure 8). Alternatively, we could assume a "zipper" model in which stems originating from opposite interface pass along each other. This would double the stem length, leading to 2.5, 3, and 3.5 stems. The experiment cannot decide between these two situations depicted in Figure 8, and various arguments can be given. (i) In the zipper model stems of half a sublayer thickness are accompanied by stems originating from the other side. Though this seems to be a difficult process in terms of reaching optimum packing, it might be facilitated by hydrogen bonds between hydroxy-terminated end groups (see also next paragraph). However, the behavior of the methyl-terminated block polymer does not seem to be different. (ii) The zipper model gains a kink energy at the expense of a loose end. This point is not expected to be decisive, as both can be estimated to be of the order of $\sim kT \ln 3$/chain. (iii) Upon cooling from 45 to 40 °C the original situation remains perfectly stable (at least over weeks). This is what one would expect rather for 5 stems that do not change into 6, but perhaps less so for 2.5 stems that could change into an integer number 3.

For the methylated sample the situation is in principle very similar (compare Figure 7), apart from a general small decrease in all spacings. This is in agreement with small-angle neutron scattering on PEO-*b*-PS samples,[29] which indicates that in the melt the structure factor of hydroxy-terminated PEO is larger than that of methylized PEO.

Comparison with PEO Homopolymer Films. Crystallization of PEO homopolymers of different weight fractions have been extensively studied.[30–32] Crystallites with an integral number of folds are more stable than other ones, and variation in supercooling results in

stepwise changes form one integrally folded state to another. However, the role of confined or even thin films has been hardly addressed. In the present context we note that in ref 31 double lamellae are reported for odd-number fold molecules in contrast to the usual situation of single lamellae for even-number folds. This is attributed to hydrogen bonding between the hydroxy end groups.[33] In the case of an odd number of folds an uneven distribution of hydrogen bonds on the fold surfaces arises, which could be avoided for double lamellae. In the present block copolymers only at one side of the crystalline PEO stem is an hydroxy group present. Assuming that again isolated end groups near the block interfaces are avoided, the double-layer structure of Figure 8 would be favorable for an even number of folds $2n$ (n integer). For a double layer with an odd number of folds $2n + 1$ non-hydrogen-bonded hydroxy groups at the block interfaces can be avoided by choosing instead a $(2n + 1)/2$ folded single layer (as pictured at the upper right part of Figure 8). These arguments do not apply, of course, to methylized PEO.

Full Model. Cooling down from the melt to the ODT (out of reach for the present compound) into the phase-separated melt, one would theoretically expect to start with polymers in a Gaussian coil conformation. Upon decreasing the temperature the scaling behavior ($L \sim \chi^{1/6}$) of the block copolymers leads to stretching of the coils and thus to a parallel preorientation. Subsequently crystallization starts, and the polymer chains continue to stretch in order to accommodate an integer or half-integer number of perpendicular stems upon folding, giving a further increase in d_{PEO}. In combination with the decreasing volume, this causes a strong lateral shrinkage of the PEO layer. Because of the linkage between the PEO and PB_h block, the latter must also stretch, and cracks are formed through the whole thickness of the films. The results do not allow a final decision between an integer and a half-integer number of stems. Arguments based on hydrogen bonding suggest an alternation between these situations for even-number and odd-number fold stems.

References and Notes

(1) Keller, A. *Faraday Discuss.* **1979**, *68*, 145.
(2) Keller, A.; Goldbeck-Wood, G. In *Comprehensive Polymer Science*, 2nd Suppl.; Aggarval, S. L., Russo, S., Eds.; Elsevier: Oxford, 1996; p 241.
(3) Strobl, G. R. *The Physics of Polymers*; Springer: Berlin, 1996.
(4) See the special issue: *Polymer* **2000**, *41*, 8751.
(5) Doye, J. P. K.; Frenkel, D. *J. Chem. Phys.* **1999**, *110*, 2692.
(6) Liu, C.; Muthukumar, M. *J. Chem. Phys.* **1998**, *109*, 2536.
(7) See for example: Hamley, I. W. *The Physics of Block Copolymers*; Oxford University Press: New York, 1998.
(8) DiMarzio, E. A.; Guttman, C. M.; Hoffman, J. D. *Macromolecules* **1980**, *13*, 1194.
(9) Whitmore, M. D.; Noolandi, J. *Macromolecules* **1988**, *21*, 1482.
(10) Vilgis, T.; Halperin, A. *Macromolecules* **1991**, *24*, 2090.
(11) Hamley, I. W. *Adv. Polym. Sci.* **1999**, *148*, 113.

(12) Hamley, I. W.; Fairclough, J. P. A.; Bates, F. S.; Ryan, A. J. *Polymer* **1998**, *39*, 1429.

(13) Mai, S.-H.; Fairclough, J. P. A.; Viras, K.; Gorry, P. A.; Hamley, I. W.; Ryan, A. J.; Booth, C. *Macromolecules* **1997**, *30*, 8392.

(14) Hamley, I. W.; Wallwork, M. L.; Smith, D. A.; Fairclough, J. P. A.; Ryan, A. J.; Mai, S.-M.; Yang, Y.-W.; Booth, C. *Polymer* **1998**, *39*, 3321.

(15) Mai, S.-M.; Fairclough, J. P. A.; Hamley, I. W.; Matsen, M. W.; Denny, R. C.; Liao, B.-X.; Y.-W.; Booth, C.; Ryan, A. J. *Macromolecules* **1996**, *29*, 6212.

(16) Zhu, L.; Chen, Y.; Zhang, A.; Calhoun, B. H.; Chun, M.; Quirk, R. P.; Cheng, S. Z. D.; Hsiao, B. S.; Yeh, F. J.; Hashimoto, T. *Phys. Rev. B* **1999**, *60*, 10022.

(17) Zhu, L.; Cheng, S. Z. D.; Calhoun, B. H.; Ge, Q.; Quirk, R. P.; Thomas, E. L.; Hsiao, B. S.; Yeh, F.; Lotz, B. *J. Am. Chem. Soc.* **2000**, *122*, 5957.

(18) Russell, T. P. *Mater. Sci. Rep.* **1990**, *5*, 171.

(19) See for example: (a) Tolan, M. *X-ray scattering from Soft-Matter Thin Films*; Springer Tracts Mod. Phys. **1999**, *148*. (b) Holý, V.; Pietsch, U.; Baumbach, T. *High-Resolution X-ray Scattering from Films and Multilayers*; Springer Tracts Mod. Phys. **1999**, *149*.

(20) REFLAN fitting program: Samoilenko, I. I.; Konovalov, O. V.; Feigin, L. A.; Shchedrin, B. M.; Yanusova, L. G. *Crystallogr. Rep.* **1999**, *44*, 310.

(21) Coulon, G.; Collin, B.; Aussere, D.; Chatenay, D.; Russell, T. P. *J. Phys. (Paris)* **1990**, *51*, 2801.

(22) Reiter, G.; Castelein, G.; Hoerner, P.; Riess, G.; Sommer, J.-U.; Floudas, G. *Eur. Phys. J. E* **2000**, *2*, 319.

(23) Hong, S.; MacKnight, W. J.; Russell, T. P.; Gido, S. P. *Macromolecules* **2001**, *34*, 2398, 2876.

(24) Almdal, K.; Rosedale, J. H.; Bates, F. S.; Wignall, G. D.; Fredrickson, G. H. *Phys. Rev. Lett.* **1990**, *65*, 1112.

(25) Hillmyer, M. A.; Bates, F. S.; Almdal, K.; Mortensen, K.; Ryan, A. J.; Fairclough, P. A. *Science* **1996**, *271*, 976.

(26) Coulon, G.; Russell, T. P.; Deline, V. R.; Green, P. F. *Macromolecules* **1989**, *22*, 2581.

(27) Russell, T. P.; Coulon, G.; Deline, V. R.; Miller, D. C. *Macromolecules* **1989**, *22*, 4600.

(28) Li, L.; Lambreva, D. M.; de Jeu, W. H. *Eur. Phys. J. E*, submitted.

(29) Frielinghaus, H.; Pedersen, W. B.; Larsen, P. S.; Almdal, K.; Mortensen, K. *Macromolecules* **2001**, *34*, 1096.

(30) Kovacs, A. J.; Straupe, C. *J. Cryst. Growth* **1980**, *48*, 210 and references therein.

(31) See references in: Cheng, S. Z. D.; Bu, H.-S.; Wunderlich, B. *Polymer* **1988**, *29*, 579.

(32) Keller, A.; Cheng, S. Z. D. *Polymer* **1998**, *39*, 4461.

(33) Shimada, T.; Okui, N.; Kawai, T. *Makromol. Chem.* **1980**, *181*, 2643.